Iranian Journal of Physics Research, Vol. 25, No. 3, 2025
DOI: 10.47176/ijpr.25.3.11628

Investigation of nonadiabatic electron dynamics effects on high-harmonic generation spectrum of H_2^+

Sajad Taghipour* and Mohsen Vafaee
Department of Chemistry, Tarbiat Modares University, PO Box 14115-175, Tehran, Iran

E-mail: sajad.taghipour@modares.ac.ir

(Received 11 January 2023; in final form 10 May 2023)

Abstract
We numerically solved the full-dimensional electronic time-dependent Schrödinger equation for H_2^+ with Born-Oppenheimer approximation under different $\sin^2$-shaped and trapezoidal laser pulses at some different wavelengths, with $I = 1 \times 10^{13}$, 3×10^{13} and 6×10^{13} Wcm^{-2} intensity at 4.73 a.u. and 7.0 a.u. internuclear distances. Some structures such as minima and oscillatory patterns appearing in the high-order harmonic generation (HHG) spectra are investigated by considering the electron localization, electron nonadiabatic dynamics, and the Rabi frequency of the population of the ground and excited electronic states to better understand the origins of these structures in the HHG spectrum. We have explored that the oscillatory pattern in the HHG spectra originates from an oscillatory pattern in the $S_g(\omega)$ and $S_u(\omega)$ (refers to recombination to the $1\sigma_g$ and $2p\sigma_u$ respectively) spectra and these oscillatory patterns in turn are due to the nonadiabatic electronic behavior appearing as a slow oscillation pattern in the ground and first excited electronic states populations. Also, we show that the minima of the HHG spectrum are related to $S_g(\omega)$, $S_u(\omega)$, $S_{gu}(\omega)$, and orbital interference.

Keywords: Half Heusler; Phase transition; dielectic function; Semiconductor; Bulk modulus; Band gap

1. Introduction

Observation of the electron dynamics requires ultrashort lasers around the attosecond time scale (~10^{-18} s) [1, 2]. Electron processes can be evaluated and modified by attaining this time resolution. One of the ways to achieve such ultra-short lasers is high-order harmonic generation (HHG). When an atom or molecule interacts with an intense laser pulse, photons with multiple of the initial fundamental frequency of the laser pulse can be generated. Such a phenomenon is called high-order harmonic generation [3]. Nowadays, HHG is the traditional way to produce spatially and temporally coherent extreme ultraviolet radiation (XUV) light, as well as light source in the attosecond regime [4]. Recently, to access to such time scale and also to apply in some fields such as control of electron wavepackets [5], molecular tomography [6], and easier access to X-rays [7], HHG has been gained much attention in the science of laser-matter interaction [4].

A simple model that allows to understand the basic features of HHG can be given by the following three-step model [3]. In the first step, the laser field distorts the Coulomb potential, so that the electron can tunnel out of the Coulomb attraction and can be free. In the second step, the ionized electron is born with zero velocity and accelerated in the laser field. When the direction of the laser field reverses, the free electron may recombine with the ion depending on the phase of the field at its birth time, and the energy is released as HHG emission (third step). At recollision, a single photon is emitted with energy $E = I_P + k$ that I_P is the ionization potential and k is the kinetic energy upon recollision. This process can repeat for each half of the laser cycle, which results in an attosecond pulse train for a laser pulse with several optical cycles [4, 8]. The HHG spectrum of molecules usually has specific structures such as sudden decrease of intensity in some harmonic orders as minima and intramolecular interference.

In this work, we numerically solve the full-dimensional electron dynamics of H_2^+ under $\sin^2$-shaped and trapezoidal laser pulses at some different wavelengths, with $I = 1 \times 10^{13}$, 3×10^{13} and 6×10^{13} Wcm^{-2} intensity at 7.0 a.u. nuclear distances (that minimum has seen and reported) and 4.73 a.u. (at this internuclear distance the coupling between the coupling between $1\sigma_g$ and $2p\sigma_u$ bound states is weaker rather than 7.0 a.u.) and derived the HHG spectra. Our focus is to uncover the origin oscillatory pattern and minima in these HHG spectra.

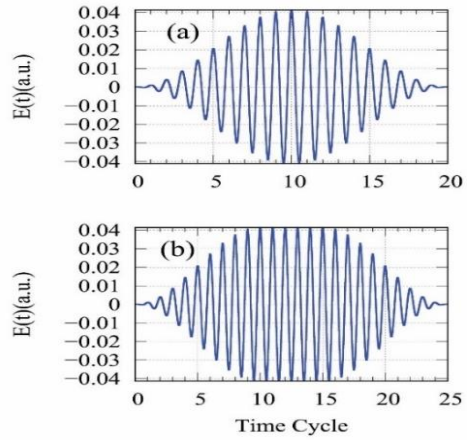

Figure. 1. (Color online) (a) The twenty-cycle $\sin^2$-shaped laser pulse with 1400 nm wavelength and of 6×10^{13} $\mathrm{Wcm^{-2}}$ intensity and (b) the 25-optical-cycle trapezoidal laser pulse with 10 cycles ramp on, 5 cycles constant, and 10 cycles ramp off (the ramps are sine-squared laser pulse).

In order to understand and identify the underlying physics behind these structures in depth, we perform an analysis of nonadiabatic electronic behavior and investigate this effect on the time-dependent population of the electronic states. Recently particular attentions have been paid to study nonadiabaticity in electron dynamics of the HHG spectra [10-13].

For describing the structure of minimum interference, theoretical [14-16] and experimental [6,17-24] studies have been performed. It is showed the minimum is dependent on the internuclear distance and orientation angle of the molecule [14, 25]. Han et al. studied the role of the internuclear distance on the interference minimum on the HHG spectrum of H_2^+ [26, 27]. They reported that when the internuclear distance is increased, contribution of recombination into the first excited state plays important role and has not been neglected and the orbital interference term also needs to be taken into account that leads to the failure of the two-center interference model.

Recently, the relationship between minimum and the transient of the electron localization on the HHG spectrum has been discussed by Miller et al [11, 12]. They argued that the minimum of HHG spectrum is related to the phase difference between the electron emission and the remained wave packet at the time of recombination [11]. They stated that non-adiabatic

dynamics is closely related to the time-dependent phase of the electron wave packet $\psi(\rho, z;\, t)$ around each nucleus [11]. They explained that at high wavelengths (such as 1400 and 1800 nm), minimum of HHG spectrum is related to the wave-packet phase (α) at the time of ionization and is not correlated with the electrons wave packet phase in the recombination time. They also expressed that when α is zero at the ionization time, the suppression would be occurred in the ionization and consequently in the generation of the HHG spectrum which leads to appear a minimum in the HHG spectrum. In contrast, when α is not zero at the ionization time, there is no suppression on the HHG spectrum [11].

In this work we seek underlying physics behind the harmonic emission in H_2^+ under relatively nonadiabatic electron dynamics. We will analysis the effect of resonance between ground and excited electronic states on the HHG spectra and investigate the role of these two lowest electronic at different internuclear distances, wavelength, intensity, and envelope of laser pulse. For study of the origin of the oscillatory patterns on the HHG spectrum, we investigate the HHG process due to the ground and first excited electronic states. The rest of the paper is organized as follows: Section 2 describes the framework for the numerical methods used to solve the time-dependent Schrödinger equation (TDSE) for H_2^+ under the laser pulses. In Section 3, simulation results are presented and discussed. Finally, Section 4 presents the conclusions. We use atomic units throughout the article unless stated otherwise.

2. NUMERICAL RESULT

Time-depended Schrödinger equation (TDSE) for a fixed-nuclei model of H_2^+ exposed to an external linearly polarized electric field can be expressed (in atomic units; $e = \hbar = m_e = 1$) as [28, 29]

$$i\frac{\partial\psi(z,\rho;\, t\,,R)}{\partial t} = H(z,\rho;\, t\,,R)\,\psi(z,\rho;\, t\,,R), \quad (1)$$

with electron cylindrical coordinate (z,ρ) which are measured with respect to the center of mass of the two nuclei (after a separation of the center-of-mass motion and ignoring molecular vibration and rotation) and R is the internuclear distance of the molecular ion. H is the total electronic Hamiltonian for H_2^+

$$H(z,\rho;\, t\,,R) = -\frac{2m_n+m_e}{4m_n m_e}\left[\frac{\partial^2}{\partial\rho^2}+\frac{1}{\rho}\frac{\partial}{\partial\rho}+\frac{\partial^2}{\partial z^2}\right] + \mathrm{V}(z,\rho;\, t\,,R), \quad (2)$$

$m_e = 1$ and m_n are the masses of electron and a single nuclei, respectively, with

$$\mathrm{V}(z,\rho;\, t\,,R) = -\frac{1}{\sqrt{\left(z+\frac{R}{2}\right)^2+\rho^2}} - \frac{1}{\sqrt{\left(z-\frac{R}{2}\right)^2+\rho^2}} + \frac{1}{R} + \left(\frac{2m_n+2m_e}{2m_n+m_e}\right) zE_0 f(t)\cos(\omega t\, +\, \varphi). \quad (3)$$

In these equations, E_0 is the laser peak amplitude, ω is angular frequency, $f(t)$ is the laser pulse envelope and φ is the carrier-envelope phase (CEP). In this work we used of the $\sin^2$-shaped laser pulse with 20 o.c. (units of "o.c." mean the optical cycle of the pulse); is shown in Fig. 1(a) and a trapezoidal pulse envelope with of time duration 25 o.c. with 10 cycles ramp on, 5 cycles constant, and 10 cycles ramp of that shown in Fig. 1(b). The TDSE is solved using unitary split-operator methods [30, 31] which the detailed numerical procedures can be found in Refs [32-34]. The finest grid size values in our numerical integration are 0.13 and 0.2, respectively for z and ρ. The size of the simulation box is chosen as $z_{\max} = 157$ and $\rho_{\max} = 124$.

The time-dependent wave function was used to obtain the power spectrum of the HHG radiation by calculating the square of the windowed Fourier transform of dipole acceleration $a_z(t)$ in the electric field direction (z) as

$$S(\omega) = \left|\frac{1}{\sqrt{2\pi}}\int_0^T \langle\psi(z\,,\ \rho;\, t,R)|a_z(t)|\psi(z\,,\ \rho;\, t,R)\rangle_{z,\rho} \times H(t)exp[-i\omega t]dt\right|^2, \quad (4)$$

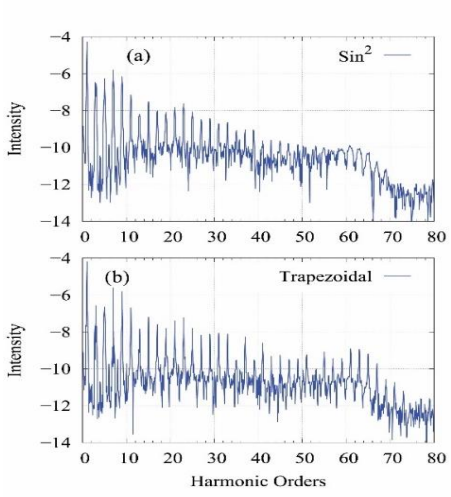

Figure. 2. (Color online) High-order harmonic spectrum for an H_2^+ at $R = 7.0$ a.u. internuclear distance under the sin^2-shaped laser field with 1400 nm wavelength and 6 ×10^{13} Wcm^{-2} intensity (Fig. 1(a) and the high-order harmonic spectrum for H_2^+ at $R = 7.0$ a.u. internuclear distances, under the trapezoidal laser field (Fig. 1(b), with 1400 nm wavelength and 6 ×10^{13} Wcm^{-2} intensity.

where

$$H(t) = 1/2[1 - cos(2\pi t/T)], \quad (5)$$

$H(t)$ is the Hanning filter and T is the total pulse duration. We use the Hanning filter to reduce the effect of unphysical features on the HHG spectrum that last after turn-off of the laser pulse. The spatial distributions of corresponding HHG spectra as a function of the electronic coordinate z, $S(z,\omega)$ is given by

$$S(z,\omega) = \left|\frac{1}{\sqrt{2\pi}}\int_0^T \langle\psi(z\ ,\ \rho;\ t,R)|a_z(t)|\psi(z\ ,\ \rho;\ t,R)\rangle_\rho \times H(t)exp[-i\omega t]dt\right|^2. \quad (6)$$

To calculate contributions of different electronic states to total HHG spectrum, $\psi(\mathrm{z},\rho;\mathrm{t},R)$ can be separate into the following components [35]:

$$\psi(\mathrm{z},\rho;\mathrm{t},R) = c_g(t)\psi_g(\mathrm{z},\rho;\mathrm{t},R) + c_u(t)\psi_u(\mathrm{z},\rho;\mathrm{t},R) + \psi_{res}(\mathrm{z},\rho;\mathrm{t},R), \quad (7)$$

where $\psi_g(\mathrm{z},\rho;\mathrm{t},R)$ and $\psi_u(\mathrm{z},\rho;\mathrm{t},R)$ refers to the wavefunctions of the ground and first excited states, respectively, corresponding to the $1s\sigma_g$ and $2p\sigma_u$ states. $\psi_{res}(\mathrm{z},\rho;\mathrm{t},R)$ is related to the residual part of total wavefuntion $\psi(\mathrm{z},\rho;\mathrm{t},R)$ containing other excited and continuum states. With substitute Eq. 7 to Eq. 4 and retain the dominant terms, we can write

$$S_{tot}(\omega) \approx S_{gu}(\omega) + 2\left[A_g^*(\omega)A_u(\omega)\right] \quad (8)$$

$$S_{gu}(\omega) = S_g(\omega) + S_u(\omega)$$

where $S_g(\omega) = \left|A_g\right|^2$, $S_u(\omega) = |A_u|^2$ and

$$A_g(\omega) = \int 2Re\langle c_g(t)\psi_g(t)|a_z(t)|\psi_{res}(t)\rangle e^{i\omega t}dt, \quad (9)$$

$$A_u(\omega) = \int 2Re\langle c_u(t)\psi_u(t)|a_z(t)|\psi_{res}(t)\rangle e^{i\omega t}dt. \quad (10)$$

In these relations, $S_g(\omega)$ and $S_u(\omega)$ refers to recombination to the $1\sigma_g$ and $2p\sigma_u$ respectively, and the term $2\left[A_g^*(\omega)A_u(\omega)\right]$ corresponds to the electronic interference term of these two localized electronic states. If $S(\omega) \approx S_{gu}(\omega)$ then the HHG spectrum includes recombination to the ground state, $S_g(\omega)$, and first excited state, $S_u(\omega)$.

In this work, the third and fourth excited electronic states are not considerably populated during the interaction and therefore the corresponding terms $S_3(\omega)$ and $S_4(\omega)$ is negligible. To study the time profile of harmonics generated, an inverse the Fourier transform over a selected range of frequencies is obtained by Morlet-wavelet transform of dipole acceleration $a_z(t)$ via [36, 37]

$$\mathrm{w}(\omega,\mathrm{t}) = \sqrt{\frac{\omega}{\sigma\pi^{\frac{1}{2}}}} \times \int_{-\infty}^{+\infty} a_z(t')\exp[-i\omega(t' - \mathrm{t})]\exp\left[-\frac{\omega^2(t'-\mathrm{t})^2}{2\sigma^2}\right]dt'. \quad (11)$$

We use $\sigma = 2\pi$ in this work.

3. RESULTS AND DISCUSSION

The high-order harmonic spectrum for the H_2^+ system, in $R = 7.0$ a. u. internuclear distance, under a 20 cycles sin^2-shaped laser field and 25 cycles trapezoidal laser pulses at 1400 nm wavelength and 6×10^{13} Wcm^{-2} intensity (shown in Fig. 1) has an interesting and special structure in the plateau which can be seen in Fig. 2. As seen in Fig. 2, there are an oscillatory behavior (maxima and minima) on the HHG spectrum. Figure 3 shows the comparison between $S(\omega)$ and $S_{gu}(\omega)$ (the sum of $S_g(\omega)$ and $S_u(\omega)$) (Fig. 3(a)), and between $S_g(\omega)$ and $S_u(\omega)$ (Fig. 3(b)), and $S_g(\omega)$ (Fig. 3(c)) and $S_u(\omega)$ (Fig.3(d)) at R=7.0 a.u. internuclear distance for the sin^2 laser field at 1400 nm wavelength with $I = 6 \times 10^{13}$ Wcm^{-2} intensity. It can be seen

that in Fig. 3(b) the oscillatory pattern on the HHG spectrum as pointed to by the solid blue and red double-arrows that related to $S_g(\omega)$ and $S_u(\omega)$, respectively. Fig. 3(a) (same as Fig. 2(a)), shows that $S_{gu}(\omega)$ is approximately equal to $S(\omega)$. Therefore, the total HHG spectrum in Fig. 3 is mostly related to the ground and the first excited electronic states, and the role of the other excited electronics states in the spectrum are negligible. For different parts of $S(\omega)$, one of these two $S_g(\omega)$ and $S_u(\omega)$ overcomes as shown in Fig. 3(b) with the blue arrows for $S_g(\omega)$ and the red arrows for S_u. It can be seen that the oscillation of $S(\omega)$ in Fig. 3(a) is related to the oscillation of the spectra of S_g and $S_{u(\omega)}$. From Fig. 4, also can see that for different parts of $S(\omega)$, this trend occurs and one of these two $S_g(\omega)$ and $S_u(\omega)$ is dominated and the oscillatory pattern in $S(\omega)$ is due to the oscillation of the spectra of S_g and S_u. Therefore, these oscillations of the of two $S_g(\omega)$ and $S_u(\omega)$ are responsible for the oscillatory patterns observed at the HHG spectra in Fig. 2. For a better representation of the oscillatory patterns and contribution of the ground and excited electronic states on the HHG spectra, $S_g(\omega) - S_u(\omega)$, the difference between S_g and S_u, is shown in Fig. 5 (a,b) that correspond to Fig. 2 .It can be seen that $S_g(\omega) - S_u(\omega)$ has clearly an oscillatory behavior. For example, Fig. 5 (a) shows that $S_u(\omega)$ for the harmonic orders between 1-13, 30-40, and 70-80 is dominated.

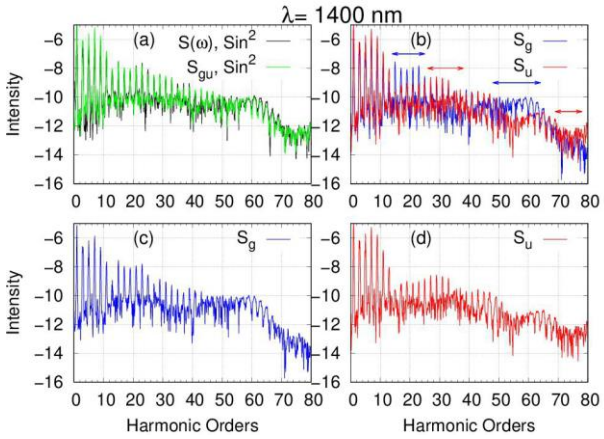

Figure. 3. (a) (Color online) The total harmonic spectrum and (b) the harmonic spectrum both of the ground and first excited electronic states. (c) The harmonic spectrum of the ground and (d) first excited electronic states for the H_2^+ in R = 7.0 a.u. internuclear distance for the $\sin^2$ laser field (Fig. 1) at 1400 nm wavelength.

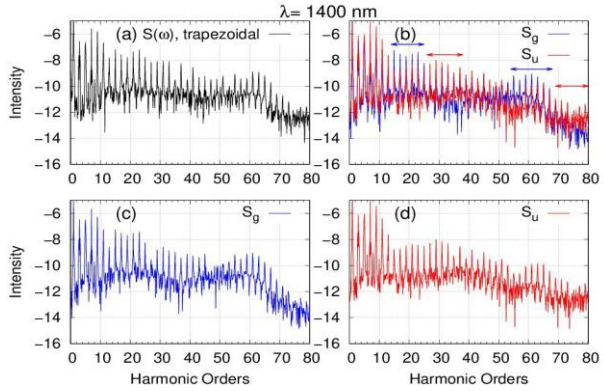

Figure. 4. (Color online) Same as Fig. 3, but for the trapezoidal laser field (Fig. 3).

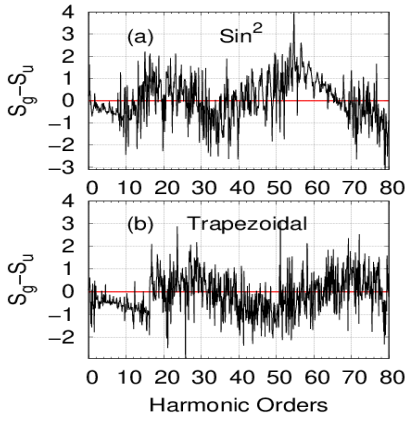

Figure. 5. (Color online) Different between the S_g and S_u ($S_g - S_u$) for H_2^+ under the $\sin^2$ and trapezoidal laser pulse at 1400 nm wavelength with $I = 6 \times 10^{13}$ Wcm^{-2} intensity.

In Figs. 6 and 7, we examine the effects of wavelength and internuclear distance on the oscillatory behavior of the HHG spectra under the $\sin^2$ and trapezoidal laser pulses. Figure 6 shows the HHG spectra for the H_2^+ system, in R=7.0 a.u. internuclear distance at 1800 nm wavelength. Comparison of Fig. 2 shows that by increasing wavelength, the cutoff position is increased.

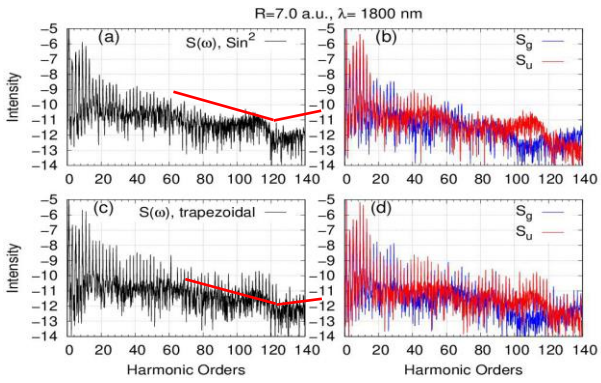

Figure. 6. (Color online) The total HHG spectrum (left panels) and the HHG spectrum due to the ground and first excited electronic states (right panels) for the $\sin^2$ and trapezoidal laser pulse for 7.0 a.u. internuclear distance at 1800 nm wavelength with $I = 6 \times 10^{13}$ Wcm^{-2} intensity.

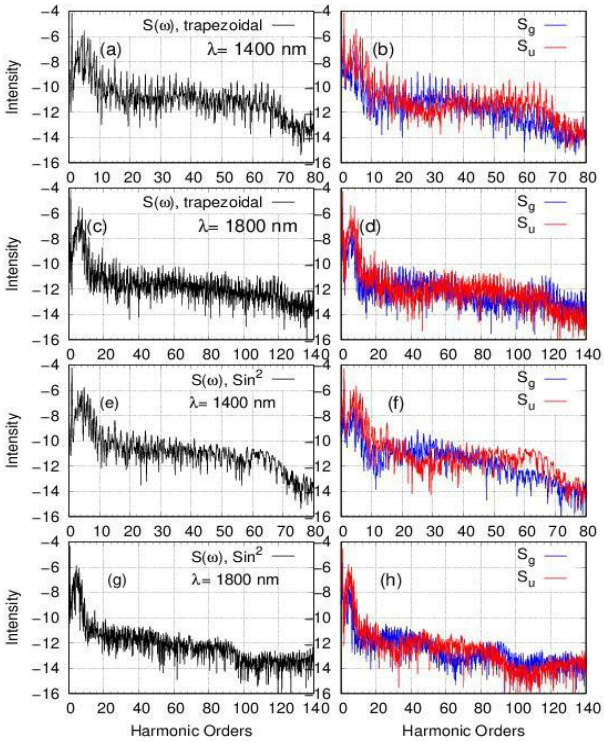

Figure. 7. (Color online) The total HHG spectrum (left panels) and the HHG spectrum of the ground and the first excited electronic states (right panels) for the $\sin^2$ and trapezoidal laser pulses with different wavelengths at ~ 4.7 a.u. internuclear distance.

However, the similar oscillatory pattern is seen on the HHG spectrum in Fig. 6. In contrast with the $R = 7.0$ a.u. where the ground and excited electron states nearly degenerate, these two states are not degenerate in the internuclear distances of 4.73 a.u. Figure 7 represents the total HHG spectrum (left panels), the HHG of the ground and the first excited states (right panels) for the $\sin^2$ and trapezoidal laser pulses at 1400 and 1800 nm wavelengths at 4.7 a.u. internuclear distances. It can be observed in all of panels have an oscillatory patterns in $S_g(\omega)$ and $S_u(\omega)$ spectrum that are similar to Fig. 6 for R=7.0 a.u. As a result, the oscillatory pattern of $S(\omega)$ spectrum are due to

the contribution of the oscillatory patterns of the ground and first excited electronic states.

To better understand the mechanism behind the oscillatory pattern and the minima in HHG, we calculated the smoothed spectra by $S_{smooth} = \int S(\tilde{\omega}) \exp(-(\tilde{\omega} - \omega)^2/\sigma^2)d\omega$ with $\sigma = 3\omega_0$ [14]. To show the coupling effects between $S_g(\omega)$ and $S_u(\omega)$, that are responsible for observing the oscillatory pattern in HHG spectra, we derived and plotted in

Fig. 8, the smoothed spectra of the $S(\omega)$, $S_{gu}(\omega)$, $S_g(\omega)$ and $S_u(\omega)$ for the sin^2-shaped and trapezoidal laser pulses (Fig. 1) at $R = 4.7$ a.u. and $R = 7.0$ a.u. internuclear distance at 1400 and 1800 nm wavelengths with $I = 6 \times 10^{13}$ Wcm^{-2} intensity. It can be seen in Figs. 8(a) and 8(b) that $S_g(\omega)$ and $S_u(\omega)$ exhibit a periodic oscillatory behavior and each of them are dominant in some parts of the HHG spectra. Figure 8 shows that with increasing the wavelength, the number of oscillations of the $S(\omega)$ is increasing.

To find out the origin of the observed the minimum in HHG spectrum, Lein *et al* reported that maxima and minima can be considered as results of the interference between two radiating point sources located at the nuclei [14]. Minima in HHG spectra also investigated by Kamta and *et al* [25]. They offer formula for the destructive interference' $N_{min}^{ti}\omega_0 = k^2/2$. In this equation, N_{min}^{ti} is the minimum order of the HHG spectrum, ω_0 is the angular frequency of the laser field, and k is the electron momentum at the instant of recombination of the electron wave packet with the ground state. After that, however, Han and *et al* [26, 27] showed at larger internuclear distance, the

two-center interference Lein's model fails. The contribution of the $S_u(\omega)$ in the two-center interference model is neglected. But, at larger internuclear distance the recombination probability of the $2p\sigma_u$ state is comparable with the $1\sigma_g$ state and the orbital interference term (the last term in equation (8)) has an important role in the minimum on the harmonic spectra [26]. Han and *et al* showed that for a 7-cycle trapezoidal laser pulse with the intensity of $I = 1.7 \times 10^{14}$ Wcm^{-2} and 800 nm wavelength and the internuclear distance at $R = 2.5$ a.u, $R = 3.8$ a.u. (small internuclear distances), the effect of the orbital interference can be ignored and the minimum position in the spectrum is approximately by the two-center interference, but for $R = 4.8$ a.u., $S_u(\omega)$ becomes dominates in the plateau region and the orbital interference leads to a minimum in the HHG spectrum [27].

Recently, at larger internuclear distances (7.0 a.u.), for a sin^2 laser pulse at 1400 (Fig. 2(a)) and 1800 nm (Fig. 6(a)) wavelengths with I= 6×10^{13} Wcm^{-2} intensity, Miller *et al.* reported that these minima are related to the nonadiabatic transient localization of the electron upon alternating nuclei [11]. Also, similar such minima can been see in Figs. 2(b), 4, 6and 7 for sin^2 and trapezoidal laser pulse at $R = 4.7$ and $R = 7.0$ a.u. internuclear distances at 1400 and 1800 nm wavelengths with $I = 6 \times 10^{13}$ Wcm^{-2} intensity. Actually, we can see a set of minima or maxima in these HHG spectra instead only one minimum order in the HHG spectra.

As we showed in Fig. 4(a) for the H_2^+ at $R = 7.0$ a.u. internuclear distance for the sin^2 laser field (Fig. 1) at 1400 nm wavelength, the $S_{gu(\omega)}$ almost is close to S. This point is clear for the smoothed spectra in Fig. 8. To evaluate contribution $S_g(\omega)$, $S_u(\omega)$, $S_{gu}(\omega)$, and orbital interference on the minimum position of the S(ω), we calculate and compare the smoothed spectra in Fig. 8. We can specify four different cases of the minima in the $S(\omega)$ spectra in this figure. *Case* (a): the orbital interference model has a good agreement with the some minima positions in Fig. 8 when the intersections between $S_g(\omega)$ and $S_u(\omega)$ is occurred. It can be seen, for example, about harmonic orders 10-20 in Fig. 8(a,b), 20-40 in Fig. 8(c,d), 38-52 in Fig. 8(e,f) and 20-40 and 80-95 in Fig. 8(g,h). *Case* (b): $S_g(\omega)$ is the determinant factor for the minima at about harmonic orders 13-19 in Fig. 8(e) and Fig. 8(f). *Case* (c): $S_u(\omega)$ is responsible for the double minima about harmonic orders 45-65, also a minimum about harmonic order 100 in Fig. 8(h). Case (d): $S_{gu}(\omega)$ is the main determinant of the location minimum of the HHG spectra such as the minima positions about harmonic order 50-100 in Fig. 8(a) , also for the minima about harmonic orders 40-80 in Fig. 8(g).

To proceed, we now investigate the relation between the oscillatory pattern in HHG spectra and the time-dependent population. Figures 9 and 10 show the time-dependent population of, respectively, the ground and first excited electronic states of the H_2^+ system at $R = 7.0$ a. u., under different duration (5, 10, 15, 20, 25, and 30 cycles) of sin^2-shaped laser pulses with the wavelength 1400 nm and $I = 6 \times 10^{13}$ Wcm^{-2} intensity shown in Fig. 11. When a system is interacting with a laser pulse, the population of the initial ground electronic state is transmitted to other electronic states or releases as electron wavepackets into the continuum states. For these laser pulses shown in Fig. 11, mainly the first two electronic states (ground and first excited electronic states) of the H_2^+ at $R = 7.0$ a. u. have population. The oscillation of the population in Figs. 9 and 10 results from the population transmission between the ground and first electronic excited states under the interaction with the laser pulse. The population starts to exchange periodically between two ground and first excited electronic states by turning on the laser pulse. As the number of cycles of the laser pulses and therefore amplitude of laser pulses increases and at near the center of the laser envelopes, the oscillation rate of the populations between the two first electronic states increases. Figures 9 and 10 show that for the all laser pulses, independent of the number of the field cycles, the population transmissions have two type oscillations; the Rabi oscillation due to coupling of the ground and first excited electronic states shown with blue lines and the slow oscillation shown with red lines. The slow oscillation is related to the variation of the Rabi frequency that in turn is due to the intensity variation during the rising and falling edge of the laser pulse.

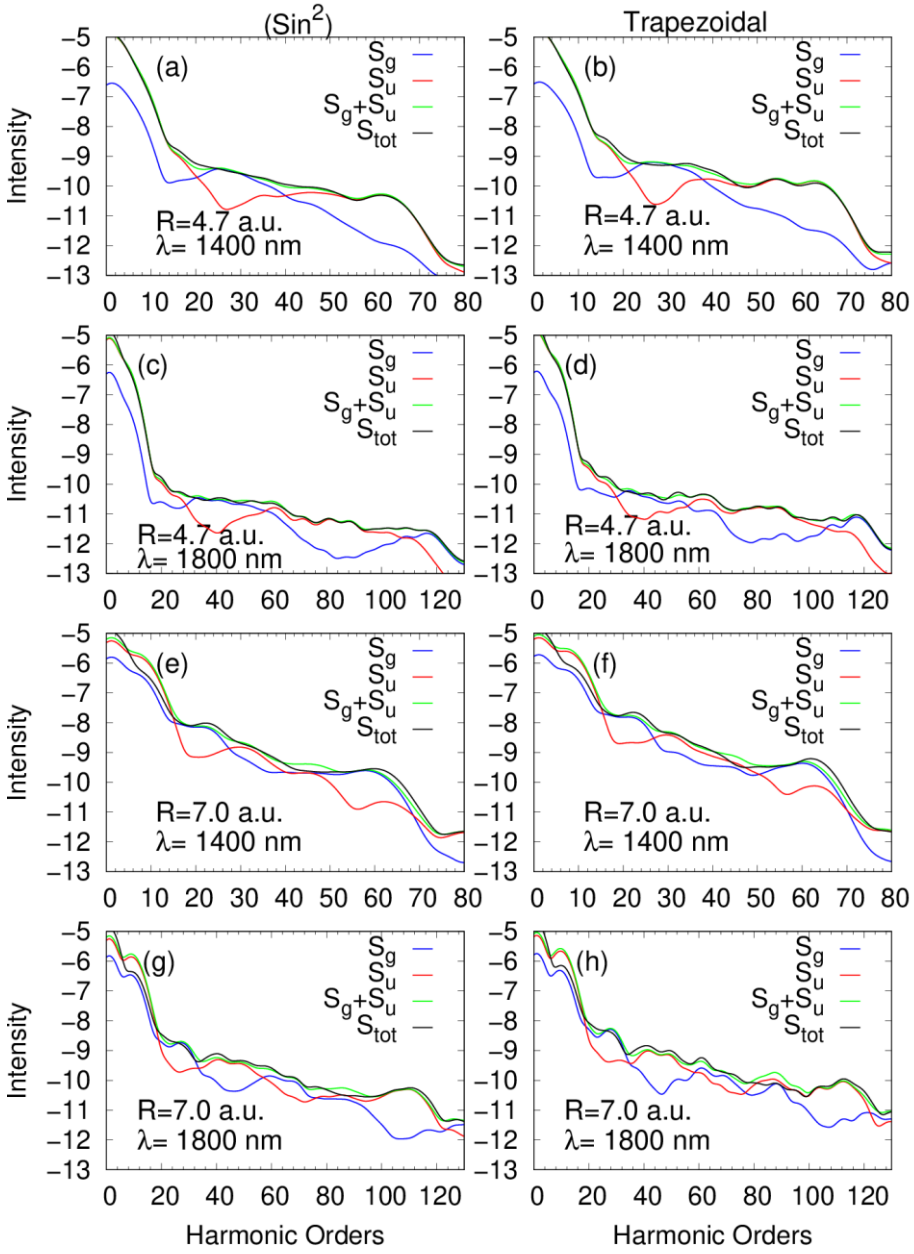

Figure. 8. The smoothed spectra of the $S(\omega)$, $S_{gu}(\omega)$, $S_g(\omega)$ and $S_u(\omega)$ for the sin^2-shaped (a,c,e,g) and the trapezoidal laser pulses (b,d,f,h) at $R = 4.7$ and $R = 7.0$ a.u. internuclear distance at 1400 and 1800 nm wavelengths with $I = 6 \times 10^{13}$ Wcm^{-2} intensity.

Our results show that the Rabi oscillation and slow oscillations also appear for the trapezoidal laser field, which we do not show here. In Figs. 9 and 10, by transition of the population to an electronic state, the probability of ionization, recombination, and therefore HHG emission increase for this state. Since the total HHG spectrum is mainly a contribution of the ground and excited states, the HHG spectrum is influenced by the smooth oscillation (red line) of the population of these two states shown in Figs. 9 and 10. This smooth oscillation of the transition of the population between the two electronic states effects both ionization/recombination rate from/to these two ground and excited electronic states which in turn affects the HHG spectrum. The effect of this smooth oscillation of the Rabi frequency appears in the oscillatory patterns of the HHG spectrum in Figs. 2, 3, 4, 6, 7 and 8. We also investigate the contribution of the ground and excited electronic states on the HHG spectra with another. The Morlet-wavelet Fourier transform of the HHG spectra of Fig. 2 is depicted in Fig. 12. Figures 12(a) and 12(b) are related to the HHG of the ground and the first excited electronic states between 8th and 12th field cycle. According to Fig. 9(d) and 10(d) can be seen the ground state has more population in duration of 8-12 optical cycles of the laser cycles. Figures 12(a) and 12(b) show that the contribution of HHG process from the ground and excited state, respectively. It can be seen in this duration of the laser field (8-12 o.c.) contribution of the ground state is more than that from the excited state. Also, according to Fig. 9(d) and 10(d) can be seen the population of the excited state ($14 < t < 16$ o.c.) is averagely more than that the ground state.

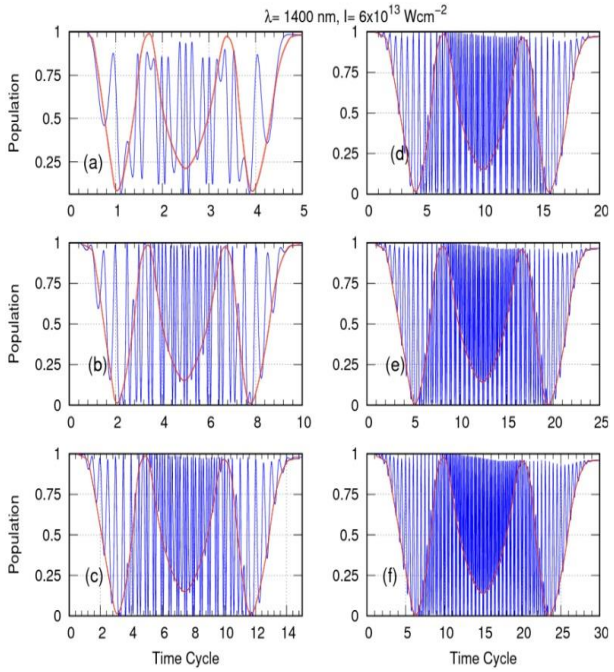

Figure. 9. (Color online) Population of the ground electronic state of H_2^+ under the interaction with the laser pulses shown in Fig. 15 with internuclear distance of 7.0 a.u. The populations are shown with blue lines that have fast oscillations with the Rabi frequency. The red lines (the pattern of the slow oscillation in the populations) are related to the Rabi frequency variations.

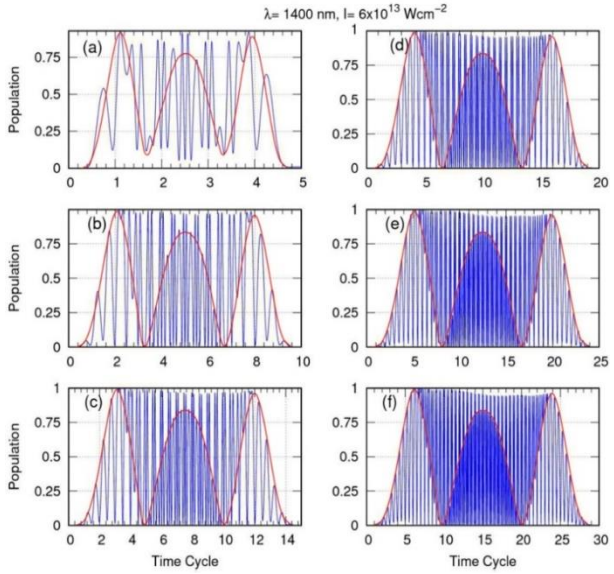

Figure. 10. (Color online) Same as Fig. 13 but for the first excited electronic state.

As a result, figure 12 shows that the in any section the contribution of the population is dominated, we can see a significant efficiency of HHG. Therefore, these periodic oscillations on the $S_g(\omega)$ and $S_u(\omega)$ lead to the oscillatory pattern of $S(\omega)$.

The Rabi frequency is the frequency of fluctuation in the populations of the two-level involved in the transition and depends on the laser intensity and wavelength [38, 39].

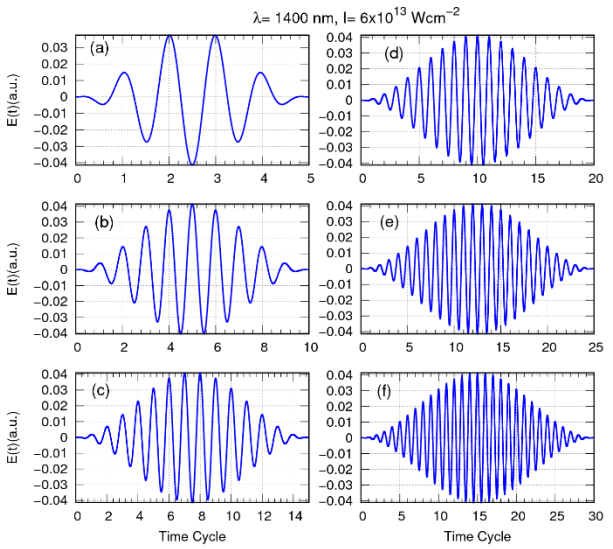

Figure. 11. (Color online) Electric field of $\sin^2$ Laser pulses with different duration at 1400 nm wavelength and 6×10^{13} Wcm^{-2} intensity used in Fig. 9 and 10.

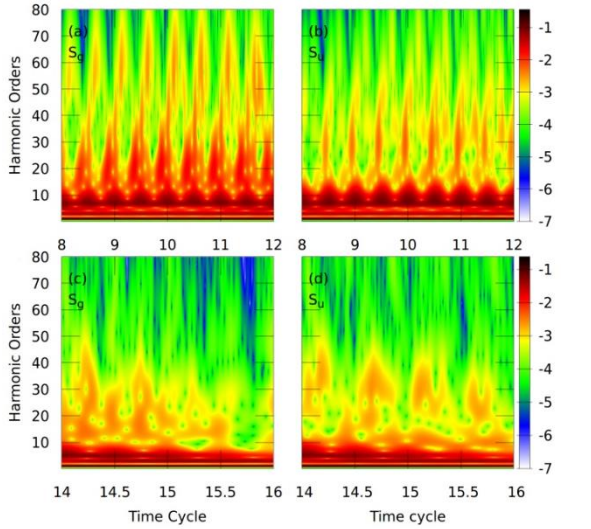

Figure. 12. (Color online) The Morlet-Violet time profiles for 20 cycle $\sin^2$ laser pulses with 1400 nm wavelength and 6×10^{13} Wcm^{-2} intensity for (a,c) the ground electronic state and (b,d) the first excited state at internuclear distances of 7.0 a.u. in different optical cycles. The HHG intensity is depicted in color logarithmic scale on the right side of panels.

For example, in Figs. 9 and 10, when the intensity is increased during the rising edge of the laser pulse, the Rabi frequency is increased. The effect of the magnitude of the intensity of the laser field on the patterns of the electron localization, the ground electronic state population, and the Rabi oscillations are represented in figure 13. This figure shows the electron wavepacket localization (a,c,e and g) and the corresponding the time-dependent population of the ground electronic state (b,d,f and h respectively) of the H_2^+ system at $R = 7.0$ a. u. internuclear distance under $\sin^2$-shaped laser pulses and trapezoidal pulse with the wavelength 1400 nm for different $I = 1 \times 10^{13}$ and $I = 3 \times 10^{13}$ Wcm^{-2} intensities.

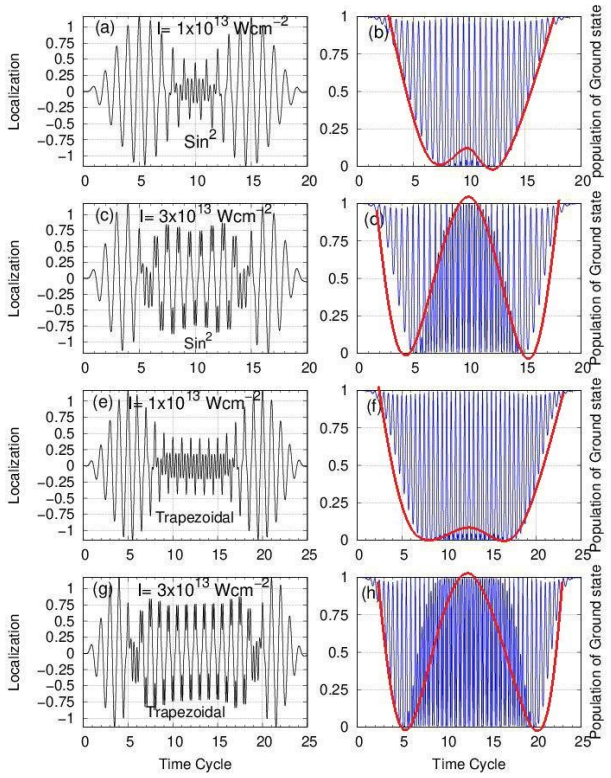

Figure. 13. (Color online) Effect of the intensity of the laser field on the patterns of the electron localization and the ground electronic state population. The electron wave packet localization (a,c,e and g) and the corresponding the time-dependent population of the ground electronic state (b,d,f and h) of the H_2^+ system at $R = 7.0$ a. u. internuclear distance under the sin^2-shaped laser pulses and the trapezoidal pulse with the wavelength 1400 nm for different 1×10^{13} and 3×10^{13} Wcm^{-2} intensities. The red lines (the pattern of the slow oscillation in the populations) are related to the Rabi frequency variations.

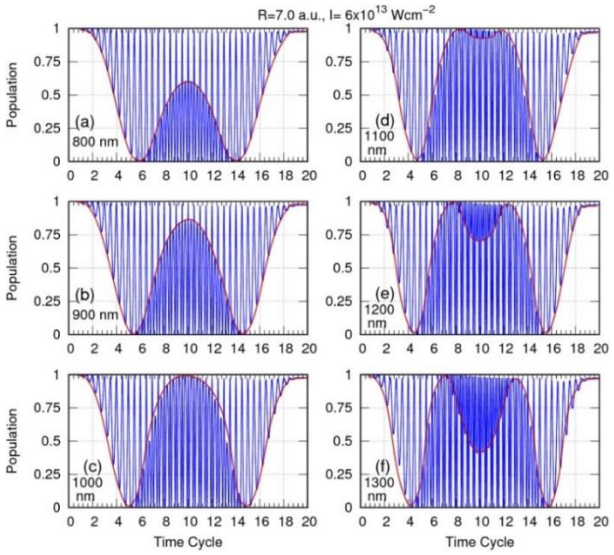

Figure. 14. (Color online) Effect of the magnitude of wavelength on the time-dependent behavior of the ground and excited states population. These figures show the time-dependent population of the ground electronic state of the H_2^+ system at $R = 7.0$ a. u. internuclear distance under sin^2-shaped laser pulses at different wavelengths (800, 900, 1000, 1100, 1200, and 1300 nm) and 6×10^{13} Wcm^{-2} intensity. The red lines (the pattern of the slow oscillation in the populations) are related to the Rabi frequency variations.

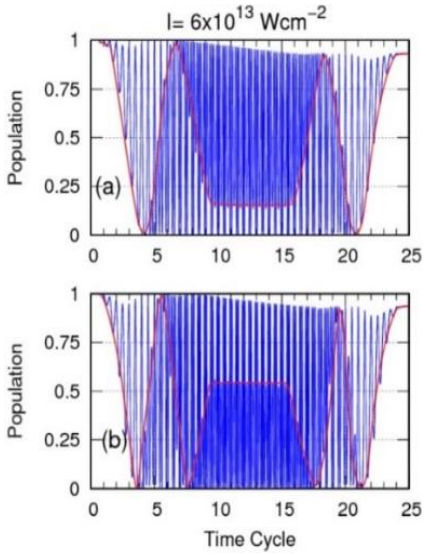

Figure. 15. (Color online) Same as Fig. 18, but for the trapezoidal laser pulses at 1400 nm (a) and 1800 nm (b) wavelengths.

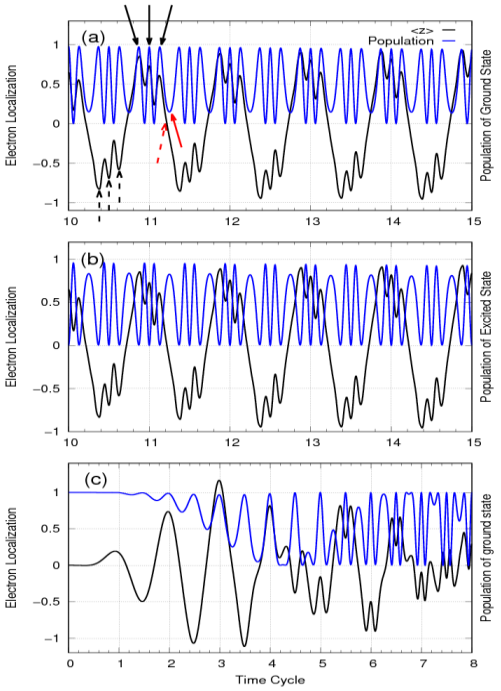

Figure. 16. (Color online) Comparison of the electron localization along the z axis (black line) with the population of the ground and excited electronic states (blue line) for the 20 cycle sin^2 laser pulses at 1400 nm wavelength and $I = 6 \times 10^{13}$ Wcm^{-2} intensity (shown in Fig. 1). It can be seen that when the electron localization is altered from one nucleus (proton) to another nucleus (marked with the red dashed arrow), subsequently a wide valley occurs in the population of the ground electronic state (marked with the red arrow). Also any triplet in the electron localization curve on each nucleus (marked with black dashed arrow) the relate a triplet peak in the population (marked with the black arrow). Similar scenario is also observed for the first excited electronic state shown in panel (b). Panel (c) shows that at the onset of nonadiabatic electronic behavior (at about 4.1 of the time cycle), singlet peaks are replaced by doublet peaks in the electron localization curve.

From the electron localization diagrams, it can be seen the electron motion remains relatively adiabatic throughout the whole driving laser pulses with $I = 1 \times 10^{13}$ Wcm^{-2} intensity as shown in Fig. 13(a) and (e) for sin^2-shaped and trapezoidal laser pulses, respectively. By increasing the driving field intensity (3×10^{13} Wcm^{-2}), the adiabatic motion of the electron wavepacket changes to a nonadiabatic motion (Fig. 13(a,c) for the sin^2 and Fig. 13(e,g) for the trapezoidal laser pulses). We observe double peaks in the nonadiabatic behavior of Fig. 13(c, g) and changes in the related Rabi frequency of the electronic state population in Fig. 13(d, h) as a slow oscillation marked with red line. It can be seen in Fig. 13 that by increasing the driving field intensity, the rate of Rabi oscillations is increased. Another point in Fig. 13 is that when the laser field amplitude is constant for example between 10-15 optical cycles in the trapezoidal laser pulse, we do not see any change in the pattern of Rabi oscillation. In other words, when laser amplitude is constant, the pattern of the Rabi oscillation in the time-dependent population of the ground electronic state does not change.

We can also investigate the effect of wavelength of the laser pulse on the time-dependent behavior of the ground and excited electronic states populations. Figure 14 shows the time-dependent population of the ground electronic state of the H_2^+ at $R = 7.0$ a. u. internuclear distance under sin^2-shaped laser pulses at different wavelengths (800, 900, 1000, 1100, 1200, and 1300 nm) and $I = 6 \times 10^{13}$ Wcm^{-2} intensity. We can see, as the wavelength increases, the nonadiabatic motion appears sooner and the Rabi frequency is increased. This effect also appears for the trapezoidal laser pulse as shown in Fig 15 for two wavelengths 1400 and 1800 nm.

Figure 16 compares the electron localization along the z axis (black line) with the population of the ground and excited electronic states (blue line) for the 20 cycle sin^2 laser pulses at 1400 nm wavelength and $I = 6 \times 10^{13}$ Wcm^{-2} intensity (shown in Fig. 1(a)). Regarding the electron localization, it can be seen that when an electron is alternated localization from one nucleus (proton) to another nucleus (marked with the red dashed arrow as an example), subsequently a wide valley occurs in the population of the ground electronic state (marked with the red arrow). For any triplet in the electron localization curve on each nucleus (marked with the black dashed arrow as an example), we can relate a triplet peak in the population (marked with the black arrow). Similar scenario is also observed for the first excited electronic state (shown in Fig. 16(b)); for any alternated localization from one nucleus to another nucleus, subsequently a wide peak occurs in the population of the ground electronic state and for any triplet in the electron localization curve, we can relate a triple valley in the population. Figure 16(c) shows that at the onset of nonadiabatic electronic behavior (at about 4.1 optical cycle), the singlet peak is replaced by doublet in the electron localization curve and we can relate these doublets in
the electron localization curve to doublet valley in the population of the ground electronic state. We can conclude that the slow variation in the Raby frequency appearing as slow oscillations pattern in the time-dependent population of the ground and first excited electronic states are due to nonadiabatic electron behavior (see Fig. 13 and 16). Therefore, it can be said that the mentioned minimum in the reports is related to the oscillations in S_g and S_u, and in turn these oscillations are due to slow oscillation patterns in the time-dependent population of the ground and first excited electronic states and consequently the nonadiabatic electron behavior.

4. CONCLUSIONS

In this work, we solved numerically the full-dimensional electronic time-dependent Schrödinger equation for H_2^+ with Born-Oppenheimer approximation under different sin^2-shaped and trapezoidal laser pulses at some different wavelengths, with $I = 1 \times 10^{13}$, 3×10^{13}, and 6×10^{13} Wcm^{-2} intensities at 4.73 a.u. and 7.0 a.u. nuclear distances and derived the HHG spectra. The minima and oscillatory patterns appeared in the HHG spectra were investigated in this work by
the electron localization, electron nonadiabatic dynamics, and the Rabi frequency to better understand the origins of these structures in the HHG spectrum.

We have shown that the oscillatory patterns of the HHG spectra are originated from the oscillatory patterns of the $S_g(\omega)$ and $S_u(\omega)$ spectra. These oscillatory patterns of the $S_g(\omega)$ and $S_u(\omega)$ spectra are due to the slow oscillation patterns in the time-dependent population of the ground and first excited electronic states that in turn are due to a nonadiabatic electronic behavior of the molecule in response to the rapid change of the laser field. In addition, in this work, we have explored how the minima emerge in the high-harmonic spectrum of H_2^+. Our results show that some minima of the HHG spectra are related to the oscillatory patterns in S_g and S_u spectra and as mentioned above these oscillatory patterns are due to nonadiabatic electronic behavior. Therefore, the appearance of some minima in the HHG spectra are due to a nonadiabatic response of the electronic wavepacket to the rapidly changing laser field. Also we detected some other minima in the HHG spectra that are related to the orbital interference.

Our simulation showed that the time-dependent population of the ground and excited electronic states show a fast oscillation corresponding to the Rabi frequency and a slow oscillation pattern corresponding to the variation of the Rabi frequency due to the intensity variation during the rising and falling edge of the laser pulse. Our results show that the both slow oscillation and Rabi oscillation appear for the both sin^2-like and trapezoidal laser field. We showed that the variation in the Rabi frequency appeared as the slow oscillation are due to the nonadiabatic electron behavior. Therefore, it can be said the some minima are related to the oscillations in $S_g(\omega)$ and $S_u(\omega)$, and in turn these oscillations are due to slow variations of the Rabi frequency and consequently the nonadiabatic electron behavior.

5. ACKNOWLEDGMENTS

We acknowledge financial support from Iran National Science Foundation: INSF with Grant No. 96015361. We are grateful to Dr. Hamed Ahmadi for his generosity and helpful discussions

References

1. T Zuo, et al. Chemical physics letters 259 (3-4) (1996) 313.
2. A D Bandrauk, Molecules in Laser Fields CRC Press (1993).
3. P B Corkum, Physical Review Letters 71(13) (1993) 1994.
4. F Krausz and M Ivanov, Reviews of Modern Physics 81(1) (2009) 163.
5. J Itatani, J Levesque, D Zeidler, H Niikura, H Pépin, J C Kieffer, P B Corkum and D M Villeneuve, Nature 432 (7019) (2004) 867.
6. J Itatani, et al., Nature 432 (7019) (2004) 867.
7. H Kapteyn, O Cohen, I Christov, and M Murnane, Science 317 (5839) (2007) 775.
8. L Gallmann, C Cirelli, and U Keller, Annual review of physical chemistry 63 (2012) 447.
9. X -B Bian and A D. Bandrauk, Physical review letters 113 (19) (2014) 193901.
10. H Ahmadi, M Vafaee, and A Maghari, Physical Review A 94 (3) (2016) 033415.
11. M Miller, A Jaroń-Becker, and A Becker, Physical Review A 93(1) (2016) 013406.
12. M Miller, A Jaroń-Becker, and A Becker, Molecular Physics 115(15-16) (2017) 1758.
13. M Uhlmann, T Kunert and R Schmidt, Journal of Physics B: Atomic, Molecular and Optical Physics 39 (14) (2006) 2989.
14. M Lein, et al., Physical Review A 66 (2) (2002) 023805.
15. M Lein, et al., Physical review letters 88 (18) (2002) 183903.
16. M Ciappina, A Becker, and A Jaroń-Becker, Physical Review A 76 (6) (2007) 063406.
17. N Wagner, et al., Proceedings of the National Academy of Sciences 103 (36) (2006) 13279.
18. W Li, et al., Science, 322 (5905) (2008) 1207.
19. S Baker et al., Physical review letters 101 (5) (2008) 053901.
20. T Kanai, S Minemoto, and H Sakai, Nature 435 (7041) (2005) 470.
21. C Vozzi, et al., Physical review letters 95 (15) (2005) 153902.
22. W Boutu, et al., Nature Physics 4 (7) (2008) 545.
23. X Zhou, et al., Physical Review Letters 100 (7) (2008) 073902.
24. C Vozzi, et al., 7 (10) (2011) 822.
25. G L Kamta and A D Bandrauk, Physical Review A 71(5) (2005) 053407.
26. Y C Han, L B Madsen, Journal of Physics B: Atomic, Molecular and Optical Physics 43 (22) (2010) 225601.
27. Y C Han and L B Madse, Physical Review A 87(4) (2013) 043404.
28. J R Hiskes, Physical Review, 122 (4) (1961) 1207.
29. M Vafaee, Physical Review A 78(2) (2008) 023410.
30. A D Bandrauk and H Shen, The Journal of chemical physics 99 (2) (1993) 1185-1193.
31. M Feit, J Fleck Jr, and A Steiger, Journal of Computational Physics 47 (3) (1982) 412.
32. M Vafaee and H Sabzyan, Journal of Physics B: Atomic, Molecular and Optical Physics 37(20) (200) 4143.
33. M Vafaee, H Sabzyan, Z Vafaee and A Katanforoush, arXiv preprint physics, 2005/0509072.
34. M Vafaee, et al., Physical Review A, 74 (4) (2006) 043416.
35. M Vafaee, H Ahmadi and A Maghari, Journal of Physics B: Atomic, Molecular and Optical Physics, 50 (2) (2016) 025601.
36. C Chandre, S Wiggins, and T Uzer, Physica D: Nonlinear Phenomena 181 (3-4) (2003) 171-196.
37. Lefebvre, C., et al., Physical Review A, 2014. 89(2) (2014) 023403.
38. P L Knight and P W Milonni, Physics Reports 66(2) (1980) 21.
39. P F Bernath, Oxford University Press, 2015.